Proc. Natl. Acad. Sci. USA
Vol. 90, pp. 7854–7858, August 1993
Biophysics

Polymer models for interphase chromosomes

(chromatin geometry/cell nucleus ultrastructure)

PHILIP HAHNFELDT†, JOHN E. HEARST‡, DAVID J. BRENNER§, RAINER K. SACHS¶‖, AND LYNN R. HLATKY†

†Joint Center for Radiation Therapy, Harvard Medical School, Boston, MA 02115; Departments of ‡Chemistry, ¶Mathematics, and ‖Physics, University of California, Berkeley, CA 94720; and §Center for Radiological Research, Columbia University, New York, NY 10032

Communicated by Berni J. Alder, May 6, 1993

ABSTRACT **The overall geometry of chromosomes in mammalian cells during interphase is analyzed. On scales larger than $\approx 10^5$ bp, a chromosome is modeled as a Gaussian polymer subjected to additional forces that confine it to a subvolume of the cell nucleus. An appropriate partial differential equation for the polymer Green's function leads to predictions for the average geometric length between two points on the chromosome. The model reproduces several of the experimental observations: (*i*) a square root dependence of average geometric distance between two marked chromosome locations on their genomic separation over genomic length scales from $\approx 10^5$ to $\approx 10^6$ bp; (*ii*) an approach of the geometric distance to a maximum value for still larger genomic separations of the two points; (*iii*) overall chromosome localization in subdomains of the cell nucleus, as suggested by fluorescent labeling of whole chromosomes and by radiobiological evidence. The model is also consistent with known properties of the 30-nm chromatin fiber. It makes a testable prediction: that for two markers a given number of base pairs apart on a given chromosome, the average geometric separation is larger if the configuration is near one end of the chromosome than if it is near the center of the chromosome.**

During the interphase part of the cell cycle, chromatin (i.e., DNA and its associated proteins) is comparatively dispersed, in contrast to its more condensed state during cell division. Chromatin geometry may have an important influence on transcription, DNA replication, cell development, and cellular response to perturbing agents such as ionizing radiation (1–3). This paper presents a mathematical polymer model for the large-scale geometric structure of chromosomes in a mammalian cell during interphase.

Extensive mathematical modeling efforts have been devoted to the physical and geometric structure of chromatin on a scale of $<10^4$ bp (1, 2, 4). Some mathematical analyses relevant to larger scales have been considered (5) but, comparatively speaking, little effort has been devoted to the very largest scales during interphase. We shall here consider scales $>10^4$ bp, emphasizing the range from $\approx 10^5$ bp up to the length of an entire chromosome—i.e., $>3 \times 10^8$ bp in the case of the largest human chromosomes (6).

Emphasizing large scales means that such comparatively well understood structures as the basic DNA double helix, and its winding onto histones to form nucleosomes (1, 2), are too small scale to be explicitly considered in our main calculation. On scales somewhat larger than the nucleosomes, chromatin is organized into a 30-nm fiber (1, 2). *Appendix 1* discusses the interrelation of the parameters of the 30-nm chromatin fiber with the parameters we shall use in the large-scale models.

The 30-nm chromatin fiber has segments that are delineated by special DNA sequences called matrix-associated regions (MARs); the term MAR refers to a possible protein matrix within the cell nucleus, whose properties are still controversial (1, 2). The segments are of variable length but on average there are somewhat $<10^5$ bp between consecutive MARs (1, 2). There is even higher-order structure, which is not well understood, organizing the segments into chromosomes (1, 2, 7). It is this higher-order structure that is our primary concern here.

Some analyses of large-scale chromosome geometry during interphase are more than a century old. But new experimental techniques have recently produced an increase in our qualitative understanding of nuclear ultrastructure (8). For example, by fluorescently "painting" a pair of homologues in a cell nucleus, it has been found that a single chromosome does not wind and twist its way throughout the entire interphase cell nucleus. Rather, at any instant, a chromosome in a mammalian cell seems to be confined to a subregion comprising, very roughly, 10% of the nuclear volume (8–12).

Less direct evidence for chromosome localization also comes from studies of ionizing radiation damage to chromosomes. An important kind of damage occurs when ionizing radiation-induced DNA double-strand breaks undergo illegitimate recombination to produce chromosome aberrations (3, 13). Because this process involves pairs of double-strand breaks, it gives information on chromosome geometry, specifically on the point-pair distribution function (essentially a geometric autocovariance function), which determines how far apart, on average, two double-strand breaks are. For example, pairs located on a single chromosome undergo pairwise interaction more often than is predicted by a model assuming complete spatial randomness, indicating some level of chromosome localization (3, 14, 15). Arguments involving the interrelation between chromosome geometry and the geometry of ionizing radiation tracks give further evidence for chromosome localization (16).

Recently, a technique has been developed for repeated measurements in different cells of the physical distance between two chosen points on one specified chromosome (17–20). This technique gives a direct measurement of the point-pair distribution function.

Thus, enough data are now accumulating to justify attempts to analyze quantitatively overall chromosome structure in interphase mammalian cells. The key question for a mathematical model is whether the higher-order structure is highly systematic and organized or has a considerable amount of randomness. In the latter case, a potentially useful approach is that of polymer physics, which models the behavior of a large, flexible linear molecule with some of its bending angles partially or wholly random (21). As long as random influences are dominant, many complications can be averaged out and surprisingly simple overall models can be obtained, even in situations in which the molecule is subjected to a complicated variety of forces.

The publication costs of this article were defrayed in part by page charge payment. This article must therefore be hereby marked "*advertisement*" in accordance with 18 U.S.C. §1734 solely to indicate this fact.

Abbreviation: MAR, matrix-associated region.

Chromosomes do show systematic interactions, constraints, and structural motifs. It is known, for example, that certain specific portions of specific chromosomes are systematically associated in the nucleolus regions, where they cooperate in the biogenesis of ribosomes (1). On the other hand, there is also evidence for considerable randomness in the ultrastructure of cell nuclei (8, 15).

Recently (20), large-scale chromosome structure during interphase was modeled by regarding chromatin as a Gaussian polymer. The model predicts that geometric separations between pairs of points on the chromosome are proportional to the square root of the genomic separations. It was found that the Gaussian polymer model works surprisingly well on scales of 10^5–10^6 bp, at least for cells prepared by the methods of van den Engh *et al.* (20). But at still larger scales, instead of continuing to increase approximately as the square root of the genomic separation, the measured geometric separations increase more slowly or become independent of genomic separations (17, 18, 20). This leveling-off effect may persist for separations up to the full length of a chromosome, from near one telomere to near the other (ref. 17; B. Trask, personal communication). The aim of the present paper is to model an interphase chromosome as a Gaussian polymer with additional constraints, thereby taking into account the observed leveling off. The models are intended to apply primarily to the time period before DNA replication (i.e., to G_1).

Polymer Models

In view of these arguments, we shall model the overall geometry of an interphase chromosome, analyzed on large scales, as a polymer (21) constrained to lie within its own nuclear subvolume, idealized as a sphere (14). Possible physical mechanisms that might induce confinement include protein tethers or the influence of other macromolecules in the nucleus.

We shall neglect many refinements in order to get a viable 0th order model. We shall calculate configuration probabilities only in thermal equilibrium. Polymer motions will not be analyzed. Only one chromosome at a time will be considered, without explicit analysis of interactions between different chromosomes or the degree to which the domains of different chromosomes may overlap.

Notation. The methods, results, and notation of the text by Doi and Edwards (ref. 21; section 2.2, section 2.3, and appendix 2.II) will be used. The chromosome is idealized as a set of $N + 1$ beads connected in order by N links. Apart from corrections for the influence of large-scale constraints, the geometric length of a single link, rather than being fixed, is determined by a Gaussian normal probability distribution, and the angle between successive links is wholly random. This approach is used because the empirical results (20) indicate that, for scales of 10^5–10^6 bp, the Gaussian polymer model applies. We could identify a bead with a MAR and/or assume that a single link corresponds to $\approx 10^5$ bp, but these identifications are not essential features of the model because all the formal calculations are invariant under appropriate rescaling of link sizes (21). We show in *Appendix 1* that Gaussian behavior at scales of 10^5–10^6 bp is consistent with known chromatin properties at smaller scales if chromatin is modeled as a worm-like coil (22–24), possibly with some additional randomness due to random angles at the locations of the MARs.

The basic configuration to be analyzed is shown in Fig. 1, where a chromosome is sketched on a scale so large the individual polymer links are not resolved. Our main goal is to calculate quantities such as the mean square physical separation $L^2 = \langle |\mathbf{R} - \mathbf{R}'|^2 \rangle$ of the points $\mathbf{R} = (X, Y, Z)$ and $\mathbf{R}' = (X', Y', Z')$ in Fig. 1; here and throughout $\langle\ \rangle$ denotes an average (over cells, at thermal equilibrium). Direct observations (17, 18, 20), with $\mathbf{R}$ and $\mathbf{R}'$ fluorescently labeled, actually are determined by two-dimensional projected distances such as $\rho = [(X - X')^2 + (Y - Y')^2]^{1/2}$. In the simple Gaussian and confinement models analyzed in the present paper, $\langle \rho^2 \rangle = (2/3)L^2$ in all cases.

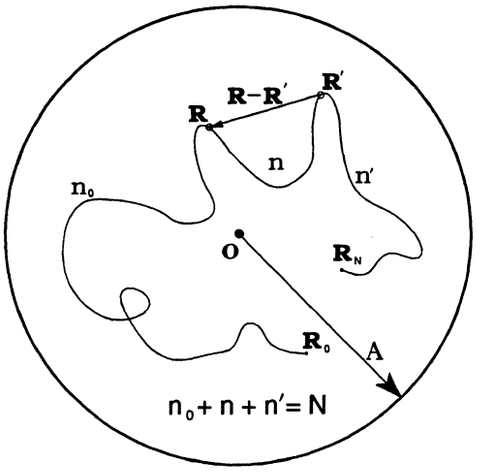

FIG. 1. Physical separations and base-pair separations. Drawing shows a chromosome, a point $\mathbf{R}$, which might be fluorescently labeled, separated by n links from a point $\mathbf{R}'$, which might be labeled a different color. The two points are, respectively, n_0 and $n' = N - n - n_0$ links from the chromosome ends (i.e., the telomeres). Circle indicates schematically a spherical subregion of the cell nucleus inside of which the chromosome is confined.

Green's Functions. We shall use the Green's function $G(\mathbf{R}_0, \mathbf{R}_N; N)$, also sometimes referred to as the "statistical weight" or "distribution function" or "partition function" (21). For an integer n' with $0 < n' < N$, the Green's function obeys a propagator equation analogous to the Kolmogorov–Chapman relation—namely (21),

$$G(\mathbf{R}_0, \mathbf{R}_N; N) = \int d\mathbf{R} G(\mathbf{R}_0, \mathbf{R}; n') G(\mathbf{R}, \mathbf{R}_N; N - n'), \quad [1]$$

where $d\mathbf{R} = dXdYdZ = R^2 d\Omega dR$. The Green's function can be used to calculate averages. For example, consider a function $f(\mathbf{R}, \mathbf{R}')$, which depends on $\mathbf{R}$ and $\mathbf{R}'$ in Fig. 1 but not on any other of the $N + 1$ bead coordinates. Then the average is (21)

$$\langle f(\mathbf{R}, \mathbf{R}') \rangle$$

$$= (1/K) \int d\mathbf{R}_0 d\mathbf{R} d\mathbf{R}' d\mathbf{R}_N\, G(\mathbf{R}_0, \mathbf{R}; n_0) G(\mathbf{R}, \mathbf{R}'; n)$$

$$G(\mathbf{R}', \mathbf{R}_N; n') f(\mathbf{R}, \mathbf{R}'). \quad [2]$$

Here K is a normalization constant, determined by

$$K = \int d\mathbf{R}_0 d\mathbf{R}_N G(\mathbf{R}_0, \mathbf{R}_N; N). \quad [3]$$

For a Gaussian polymer the Green's function (21) is

$$G(\mathbf{R}, \mathbf{R}'; n) = \left[\frac{2\pi n b^2}{3} \right]^{-3/2} \exp\left[- \frac{3(\mathbf{R} - \mathbf{R}')^2}{2nb^2} \right], \quad [4]$$

where b is the rms geometric length of one link. A calculation using Eq. 2, Eq. 4, and $L^2 = \langle |\mathbf{R} - \mathbf{R}'|^2 \rangle$ gives

$$K = 1, \qquad L^2 = nb^2. \quad [5]$$

Thus, in the Gaussian case, geometric lengths are proportional to the square root of the genomic distance—i.e., $L \propto n^{1/2}$.

Spherical Confinement. As discussed above, the Gaussian polymer model breaks down for base-pair separations larger than $\approx 10^6$. Therefore, suppose that, in addition to its contour linkage, supplied by harmonic forces between successive beads, the polymer is confined within a sphere of radius A by forces localized at the surface of the sphere. In an appropriate continuum limit, which we henceforth adopt, N, n, and n_0 are treated as continuous variables and the problem of finding the Green's function $G(\mathbf{R}, \mathbf{R}'; n)$ reduces (21) to solving, for $n > 0$, a familiar initial-value, boundary-value problem for the diffusion equation, as follows:

$$\left[\frac{\partial}{\partial n} - \frac{b^2}{6}\frac{\partial^2}{\partial \mathbf{R}^2}\right] G(\mathbf{R}, \mathbf{R}'; n) = 0, \qquad [6]$$

where $G(\mathbf{R}, \mathbf{R}', 0) = \delta(\mathbf{R} - \mathbf{R}')$ and $[G]_{|\mathbf{R}|=A} = 0$. Here $\partial^2/\partial \mathbf{R}^2$ is the Laplacian and δ is the three-dimensional Dirac δ function.

Solutions. The solution of Eq. **6**, and some applications to polymer physics, are well known (25–27). By standard superposition (25)

$$G = \sum_{lmi} \frac{\Psi^*_{lmi}(\mathbf{R})\Psi_{lmi}(\mathbf{R}')}{A_{li}} \exp[-k_{li}n], \qquad [7]$$

where $l \geq 0$, $|m| \leq l$, $i \geq 1$; $\Psi_{lmi}(\mathbf{R}) = Y_{lm}(\theta, \phi)\chi_{li}(R)$; $A_{li} = \int R^2 dR |\chi_{li}|^2$; Y_{lm} denotes a spherical harmonic; radial integrals, such as the integral in Eq. **7**, always have limits 0, A; and $\chi_{li}(R)$ is a radial eigenfunction with eigenvalue k_{li}. In terms of the lth spherical Bessel function, j_l, and its ith ordered zero κ_{li} we have (25):

$$\chi_{li}(R) = j_l(\kappa_{li}R/A); \qquad j_l(\kappa_{li}) = 0; \qquad k_{li} = \kappa_{li}^2 b^2/(6A^2). \qquad [8]$$

In the cases of interest to us, $A \gg b$. In the limit $A \to \infty$, solving Eq. **6** gives the function G in Eq. **4**—i.e., this case is the Gaussian polymer already analyzed.

Results

Appendix 2 gives details on evaluating averages, using the Green's function and Eq. **2**. This section presents some graphs on averages and a comparison to empirical data.

We shall regard the number of links n between $\mathbf{R}$ and $\mathbf{R}'$ in Fig. 1 as the basic independent variable. In the Gaussian case, Eq. **5** shows that L^2 is independent of the polymer configuration outside the genomic stretch of interest—i.e., independent of n_0 and n' in Fig. 1. In the spherical confinement case, there is a weak dependence on n_0 and n' but the main dependence is still on n. Consequently, we consider extreme values of n_0 and n'; intermediate cases are easily estimated from the extreme ones. One extreme case for n_0 is $n_0 = 0$, corresponding to a situation where $\mathbf{R}$ is very near a chromosome telomere (Fig. 1). The other limit is n_0 large, specifically $n_0 k_{01} \gg 1$, where $k_{01} = \pi^2 b^2/(6A^2)$ is the smallest eigenvalue in Eq. **8**. For $n_0 k_{01} \gg 1$, L^2 is independent of n_0 (see *Appendix 2*). Considering also the two extreme cases for n' we get three nonequivalent cases: $n_0 = 0 = n'$; $n_0 = 0$, $n'k_{01} \gg 1$; and $n_0 k_{01} \gg 1$, $n'k_{01} \gg 1$.

Fig. 2 shows the results for these cases. For "small" genomic separations—i.e., for $nk_{01} \ll 1$, the behavior is similar to that of a corresponding Gaussian polymer (curve d), and for larger n the curves show the leveling off observed (17, 18, 20) experimentally.

More specifically, the data of van den Engh *et al.* (20) concerns a 6-Mbp region very near one end of human chromosome 4. Using the Green's function for the case $n_0 = 0$, $n'k_{01} \gg 1$ and fitting an appropriate theoretical average to the data by adjusting A and b give the curve shown in Fig. 3. The inferred values for b and A are considerably larger than

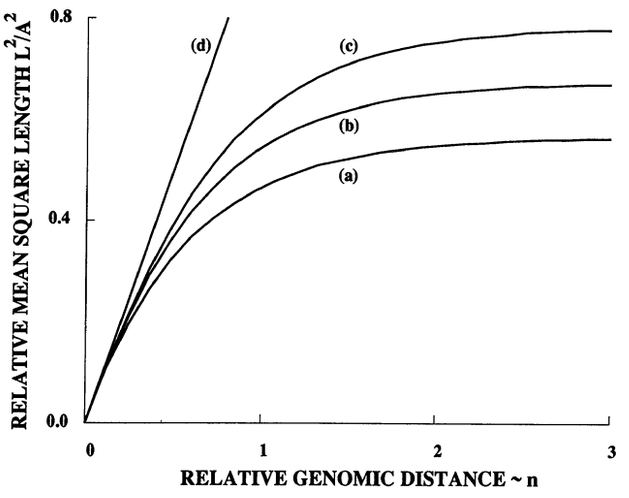

FIG. 2. Predicted values of interphase separations. In the models, average physical distance is a function of genomic distance, and genomic distance can be taken as $10^5 n$ bp, where n is the number of links. Horizontal axis is nb^2/A^2—i.e., n rescaled by using the rms length b of one link for a corresponding, unconstrained Gaussian polymer and using the radius A of the confining sphere for the chromosome. Vertical axis is the predicted mean square distance, $L^2 = \langle |\mathbf{R} - \mathbf{R}'|^2 \rangle$, in units of A (see Fig. 1). Here $\langle\ \rangle$ denotes an average. Curve a, curve for $n_0 k_{01} \gg 1$, $n'k_{01} \gg 1$, appropriate for a configuration near the middle of a long chromosome (see text). Curve b, curve for $n_0 = 0$, $n'k_{01} \gg 1$, appropriate for a configuration near one telomere of a long chromosome. Curve c, curve for $n_0 = 0 = n'$, appropriate for a chromosome whose entire length is n links. The height at which the curve levels off is a measure of the chromosome domain size. Cases intermediate between curves a and b, or b and c, have intermediate curves (not shown). Curve d, line for a corresponding Gaussian polymer without confinement.

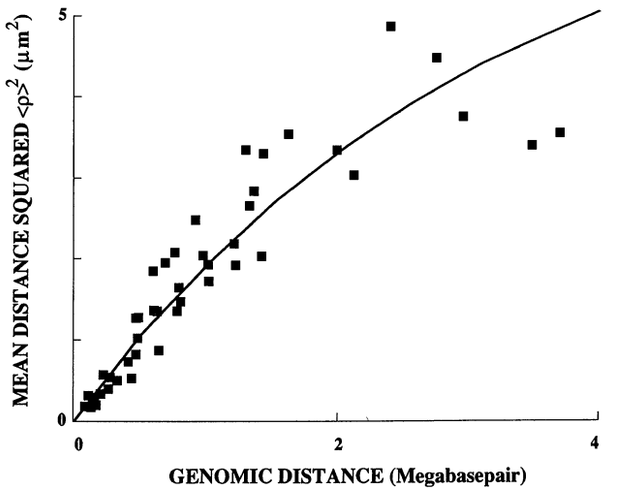

FIG. 3. Comparing model and experiment. Data points are from van den Engh *et al.* (20). The curve is obtained from the model assuming a measured distance is a two-dimensional projection $\rho = [(X - X')^2 + (Y - Y')^2]^{1/2}$ and averaging (see *Appendix 2*). Parameters A and b were adjusted to give the best fit to the data; $A \approx 6.3$ μm. Assigning the nominal value of 10^5 bp to one link gives $b \approx 0.6$ μm. Results for other nominal values can be obtained from the scale invariance of the formalism—i.e., $10^5 \to K \times 10^5$ corresponds to $b \to K^{1/2}b$ and $A \to A$. Numerical values ($A \approx 6.3$ μm, $b \approx 0.6$ μm) apply to slides prepared from cells swollen in suspension (18, 20).

would be found in a live cell, owing to the slide preparation procedure, which includes hypotonic swelling (18, 20).

Discussion

The success of the polymer models in the range $\approx 10^5$ to $\approx 10^6$ bp (20) is evidence that over such scales there is indeed considerable randomness. We have shown (Fig. 2) that a simple confinement polymer model can account for the observed leveling off of physical separations at still larger genomic separations. There are two essential adjustable parameters (Fig. 3) and these suffice to give reasonable fits to the published data. The parameters are consistent with the structure of DNA and chromatin on the level of the 30-nm fiber (see *Appendix 1*).

The confinement model predicts that, for a given genomic separation (n links in Fig. 1), the physical separations are larger for a configuration near the end of a chromosome than for a configuration near the middle of a chromosome. Intuitively speaking, there is very low probability of finding a point on the chromosome near the confining surface, since a configuration with that point on the surface would have low entropy (due to the systematic location of all nearby points on the same side—namely, the inside—of the surface). Similarly, given a stretch of n links, it tends to be closer to the center, and thus also shorter, if there are two long tails flanking the stretch—i.e., if n_0 and n' in Fig. 1 are large.

For the end points of a chromosome, the rms separation, read off the asymptote in Fig. 2 (curve c), is $\approx 0.885A$ where A is the confining sphere radius. This value can be compared to the separation of two points located at random within the confining sphere. The probability that two randomly located points are a distance r or less apart is (28) $F(y) = 8y^3 - 9y^4 + 2y^6$, where $y = r/2A$. The mean square distance is consequently $(2A)^2 \int_0^1 y^2 F'(y) dy = 1.2A^2$, corresponding to a rms separation of $\approx 1.1A$—i.e., a somewhat larger separation in the random case than in the polymer case, even for a value of n so large that the asymptote in curve c of Fig. 2 is attained.

Confinement of the kind we have modeled could occur in various ways. There might be one or more organizing center(s) for each chromosome, with protein tethers to some locations on the chromosome. Alternatively, the overall excluded volume influence of other macromolecules within the cell nucleus could induce confinement.

The current model does not specify the extent to which different chromosomes intertwine. However, the value of A derived in Fig. 3 corresponds to considerable overlapping, consistent with fluorescent *in situ* hybridization studies (8, 10–12) and radiobiological evidence (3, 14).

A realistic geometric model of the large-scale structure of chromosomes would have many applications. In particular, analyzing chromosomal aberrations formed by pairwise interactions of ionizing radiation-produced DNA double-strand breaks requires considerable geometric detail (16). It also requires some knowledge of chromatin motion, since it is known (14, 16, 29) that the pairwise interactions are not well mixed. An attractive feature of polymer models for radiobiological applications is that each model for the average geometry at thermal equilibrium automatically implies a dynamic model with which to estimate chromatin motion (21).

Various generalizations of our results are possible—e.g., to confining domains having cylindrical rather than spherical symmetry or to confinement achieved by conservative forces rather than rigid walls (21, 26, 27).

To summarize, we have suggested that polymer models may be capable of predicting the main features of large-scale interphase chromosome geometry. If so, the simplifications obtained by averaging out details will be significant in a variety of applications, including radiobiology. Further experiments on point-pair distributions, of the kind developed by Trask and coworkers (17–20), should help determine the appropriate intermixture of systematic and random structural motifs, leading to refinement of the models.

Appendix 1: Worm-Like Coils

A Gaussian polymer is a convenient way to approximate, for large scales, the behavior of a worm-like coil (22, 23). Presumably, however, a worm-like coil model for chromatin based on the 30-nm fiber as the basic structure gives a more realistic detailed picture. Here we outline the relation between these two pictures.

The thermal equilibrium properties of a worm-like coil are specified by its persistence length a and by its contour length L_c (22–24). In our notation, the contour length is given by $L_c = 10^5 n/\nu$ μm, where we have used the same nominal value of base pairs per link as before and ν is the number of base pairs per micrometer. The persistence length of the 30-nm fiber is not known but can be estimated from the value of $b \approx 0.6$ μm found in Fig. 3 by using the standard equation (22, 24) $L^2 = 2aL_c[1 - (a/L_c)(1 - e^{-a/L_c})]$. For the straight line portion of the curve in Fig. 3, this becomes $nb^2 \approx 2aL_c = 10^5 an/\nu$—i.e., $a \approx 1.8 \times 10^{-6}\nu$ μm. For the 30-nm fiber in a live cell, $\nu \approx 1.2 \times 10^5$ bp/μm (1, 2) and we get $a \approx 0.22$ μm, corresponding to $\approx 2.6 \times 10^4$ bp. More generally, since the slide preparation involves a swelling step, we can take for the 30-nm fiber $\nu = 1.2 \times 10^5/f$, where f is a linear swelling factor, which might be in the range 1–3. Then the argument gives $a \approx 0.22/f$ μm, corresponding to $\approx 2.6 \times 10^4/f^2$ bp and a has the same order of magnitude as the persistence length of DNA itself, without associated proteins, which is ≈ 0.060 μm (30, 31). The stiffness is then also comparable, since persistence length is proportional to stiffness [the proportionality constant depending on the temperature (32) and, for DNA, on the salt concentration (33)], which is reasonable given the structure of the 30-nm fiber.

The estimated statistical length $2a$ corresponds to $<10^5$ bp, as is required (21–24) for the observed near-Gaussian behavior in Fig. 3 at scales of 10^5–10^6 bp. It could be that other small-scale models of chromatin—e.g., the nucleosome, "beads-on-a-string" model, or a model that has random angles at the MARs—are more appropriate for the experimental conditions of interest. However, in such cases the statistical length in base pairs is even smaller than that estimated above, so the argument suffices to show that our Gaussian assumption about the chromosome structure at a scale of 10^5 bp is consistent with standard information about smaller scales.

Appendix 2: Averages

Given the series from (Eqs. 7 and 8) for the Green's function, averages can be computed, as we now illustrate. Suppose that, in Fig. 1, $n_0 = 0$—i.e., the point $\mathbf{R}$ is very near a telomere. Then calculating $\langle |\mathbf{R} - \mathbf{R}'|^2 \rangle$ involves calculating $\langle R^2 \rangle$, $\langle R'^2 \rangle$, and

$$\langle \mathbf{R}\cdot\mathbf{R}' \rangle = \frac{1}{K} \int d\mathbf{R}\, d\mathbf{R}'\, d\mathbf{R}_N\, G(\mathbf{R}, \mathbf{R}'; n) G(\mathbf{R}', \mathbf{R}_N; n')\, \mathbf{R}\cdot\mathbf{R}'. \quad [9]$$

This expression can be evaluated by Eqs. 3, 7, 8, and standard properties (25) of spherical harmonics and spherical Bessel functions to obtain:

$$\langle \mathbf{R}\cdot\mathbf{R}' \rangle = \frac{4\pi}{K} \sum_{ij} D_i F_{ij} B_j \frac{e^{-nk_{1i} - n'k_{0j}}}{A_{1i} A_{0j}},$$

where

$$K = 4\pi \sum_{j=1}^{\infty} \frac{B_j^2 \exp[-k_{0j}(n+n')]}{A_{0j}},$$

$$A_{0j} = A^3/(2j^2\pi^2),$$

$$A_{1i} = A^3 \sin(\kappa_{1i})^2/(2\kappa_{1i}^2),$$

$$B_j = \int \chi_{0j} R^2 dR = (-1)^{j+1} A^3/(\pi j)^2, \qquad [10]$$

$$D_i = -A^4 \sin\kappa_{1i}/\kappa_{1i}^2,$$

$$F_{ij} = 2(-1)^{j+1} A^4 \sin\kappa_{1j}/(\kappa_{1j}^2 - \pi^2 i^2)^2.$$

Eqs. **10** can be evaluated numerically. The code needed is very simple and runs rapidly even on a workstation.

If we need the limit of Eqs. **10** for n' large, we merely drop all terms in the series of Eqs. **10** except terms involving the factor $\exp[-n'k_{01}]$. Then the n' dependence cancels between the numerator and denominator of Eqs. **10** for $\langle \mathbf{R}\cdot\mathbf{R}' \rangle$—i.e., for n' sufficiently large, the average $\langle \mathbf{R}\cdot\mathbf{R}' \rangle$ is independent of n'.

The remaining quantities needed to calculate L^2, for the various cases discussed in Fig. 2, can be calculated by wholly analogous manipulations and Fig. 2 presents the main results.

Calculating $\langle \rho \rangle$ for Fig. 3 is slightly more difficult, because ρ involves a square root. We proceeded as follows. For $nk_{01} \ll 1$, the Gaussian limit, Eq. **4**, applies and a direct integration gives $\langle \rho \rangle^2 = (\pi/4)\langle \rho^2 \rangle = (2/3)(\pi/4)L^2$, where L^2 can be calculated as discussed above. In the opposite limit—i.e., $nk_{01} \gg 1$—only the leading term ($l = 0 = m$, $i = 1$) in the series expansion (Eq. **7**) for the Green's function $G(\mathbf{R}, \mathbf{R}', n)$ need be retained, by an argument similar to that given above. Evaluating the leading term in the average reduces to computing the integral

$$\int_0^1 dr \int_0^1 dr' \int_0^{\pi} d\theta \int_0^{\pi} d\theta' \int_0^{2\pi} d\zeta\, ss'$$

$$[s^2 + s'^2 - 2ss'\cos\zeta]^{1/2} \sin(\pi r)\sin(\pi r'), \qquad [11]$$

where $s = r\sin\theta$. This integral apparently cannot be evaluated analytically. It was performed numerically, using an adaptive technique involving a one-dimensional method in each dimension (34). The result is that in this limit $\langle \rho \rangle^2 \approx (2/3)(0.805)L^2$. We then interpolated between the two limits by interpolating between the two factors $\pi/4 \approx 0.785$ and 0.805; the interpolation was checked by evaluating, also by numerical integration, the next two terms in the expansion of the Green's function $G(\mathbf{R}, \mathbf{R}', n)$ for large n. The results are presented in Fig. 3.

We are grateful to G. van den Engh, C. Schmid, and B. Trask for useful suggestions and discussions. This research was supported in part by National Institutes of Health Grants CA-44669 and GM-41911, National Science Foundation Grant DMS 9025103, and National Cancer Institute Grant CA-12536.

1. Van Holde, K. E. (1989) *Chromatin* (Springer, New York).
2. Wolffe, A. (1992) *Chromatin: Structure and Function* (Academic, San Diego).
3. Savage, J. R. K. (1990) in *Mutation and the Environment: Progress in Clinical and Biological Research*, eds. Mendelsohn, M. & Albertini, R. J. (Wiley-Liss, New York), Vol. 340B, pp. 385–396.
4. Vologodskii, A. V. (1992) *Topology and Physics of Circular DNA* (CRC Press, Boca Raton, FL).
5. Selvin, P. R., Scalettar, B. A., Langmore, J. P., Axelrod, D., Klein, M. P. & Hearst, J. E. (1990) *J. Mol. Biol.* **214,** 911–922.
6. Morton, N. E. (1991) *Proc. Natl. Acad. Sci. USA* **88,** 7474–7476.
7. Adolph, K. W. (1990) *Chromosomes: Eukaryotic, Prokaryotic, and Viral* (CRC Press, Boca Raton, FL), Vol. 1.
8. Haaf, T. & Schmid, M. (1991) *Exp. Cell Res.* **192,** 325–332.
9. Agard, D. A. & Sedat, J. W. (1983) *Nature (London)* **302,** 676–681.
10. Lichter, P., Cremer, T., Borden, J., Manuelidis, L. & Ward, D. C. (1988) *Hum. Genet.* **80,** 224–234.
11. van Dekken, H., Pinkel, D., Mullikin, J., Trask, B., van den Engh, G. & Gray, J. (1989) *J. Cell Sci.* **94,** 299–306.
12. Manuelidis, L. (1990) *Science* **250,** 1533–1540.
13. Hahnfeldt, P., Sachs, R. K. & Hlatky, L. R. (1992) *J. Math. Biol.* **30,** 493–511.
14. Hlatky, L., Sachs, R. K. & Hahnfeldt, P. (1992) *Radiat. Res.* **129,** 304–308.
15. Sachs, R. K., Awa, A., Kodama, Y., Nakano, M., Ohtaki, K. & Lucas, J. N. (1993) *Radiat. Res.* **133,** in press.
16. Brenner, D. J. (1988) *Radiat. Environ. Biophys.* **27,** 189–199.
17. Trask, B., Pinkel, D. & van den Engh, G. (1991) *Genomics* **5,** 710–717.
18. Trask, B. J., Massa, H., Kenwrick, S. & Gitschier, J. (1991) *Am. J. Hum. Genet.* **48,** 1–15.
19. Brandriff, B. F., Gordon, L. A. & Trask, B. J. (1991) *Environ. Mol. Mutagenesis* **18,** 259–262.
20. van den Engh, G., Sachs, R. & Trask, B. (1992) *Science* **257,** 1410–1412.
21. Doi, M. & Edwards, S. F. (1988) *The Theory of Polymer Dynamics* (Oxford Univ. Press, Oxford).
22. Kratky, O. & Porod, G. (1949) *Rec. Trav. Chim.* **68,** 1106.
23. Hearst, J. E. & Stockmayer, W. H. (1962) *J. Chem. Phys.* **37,** 1425–1433.
24. Cantor, C. R. & Schimmel, P. R. (1980) *Biophysical Chemistry* (Freeman, New York), Chap. 18 and 19, pp. 979–1039.
25. Morse, P. M. & Feshbach, H. (1953) *Methods of Theoretical Physics* (McGraw-Hill, New York).
26. Cassasa, E. F. & Tagami, Y. (1969) *Macromolecules* **2,** 14–26.
27. Napper, D. H. (1983) *Polymeric Stabilization of Colloidal Dispersions* (Academic, London).
28. Kendall, M. G. & Moran, P. A. P. (1963) *Geometrical Probability* (Griffin, London), pp. 53–54.
29. Brenner, D. J. (1990) *Radiat. Res.* **124,** S29–S37.
30. Schmid, C. W., Rinehart, F. P. & Hearst, J. E. (1971) *Biopolymers* **10,** 883–893.
31. Hearst, J. E. & Reese, D. A. (1980) *J. Chem. Phys.* **73,** 3007–3009.
32. Gray, H. B. & Hearst, J. E. (1968) *J. Mol. Biol.* **35,** 111–129.
33. Rinehart, F. P. & Hearst, J. E. (1972) *Arch. Biochem. Biophys.* **152,** 723–732.
34. Atkinson, K. (1978) *An Introduction to Numerical Analysis* (Wiley, New York).